

# Design and Optimization of a Five-Finger Haptic Glove Mechanism

Zhou Ma

Robotics and Mechatronics Lab,  
Department of Mechanical and  
Aerospace Engineering,  
The George Washington University,  
801 22nd Street, North West,  
Washington, DC 20052

Pinhas Ben-Tzvi

Robotics and Mechatronics Lab,  
Department of Mechanical and  
Aerospace Engineering,  
The George Washington University,  
801 22nd Street, North West,  
Washington, DC 20052  
e-mail: bentzvi@gwu.edu

*This paper describes the design and optimization of a novel five-finger haptic glove mechanism, which uses a worm-gear motor and an antagonistically routed cable mechanism at each finger as both active and passive force display actuators. Existing haptic gloves either restrict the natural motion and maximum output force of the hand or are bulky and heavy. In order to tackle these challenges, the five-finger haptic glove is designed to minimize the size and weight and maximize the workspace and force output range of the glove. The glove is a wireless and self-contained mechatronic system that mounts over the dorsum of a bare hand and provides haptic force feedback to each finger. This paper describes the mechatronic design of the glove and the method to optimize the link length with the purpose of enhancing workspace and the force transmission ratio. Simulation and experimental results are reported, showing the future potential of the proposed system in haptic applications and rehabilitation therapy. [DOI: 10.1115/1.4029437]*

## 1 Introduction

Haptic interfaces have greatly augmented immersive reality sensing beyond the senses of sight and hearing [1]. Using three stimuli—visual, auditory, and haptic—it is possible to generate many desired environments in a believable and immersive manner [2]. For tasks requiring more dexterity, such as telemanipulation, it may be necessary to control applied forces on independent fingers rather than at the wrist, as joysticks and master arms do [3]. One kind of haptic device, the haptic glove, is worn on the user's hand and provides force feedback to the fingers. This type of mechanism improves force feedback by allowing the user to “feel” virtual objects in a more natural way. This ability is required in many applications such as virtual reality [4], tele-operation [5], human-assistive devices [6], and medical applications [7]. The high dexterity of haptic gloves also makes them applicable to the control of complex movements of remote robots, as opposed to other haptic devices such as joysticks and PHANTOM [8].

A haptic glove should have two basic functions: (1) to measure the kinematic configuration (position, velocity, acceleration) and contact forces of the user's hand and (2) to display contact forces and positions to the user [9]. However, due to the human hand's dexterity and complex anatomy, physiology and sensory structures [10,11], designing a haptic glove to match the hand's dexterity and to provide force feedback for grasping and manipulating objects of varying sizes and weights is not an easy task.

As a force feedback user interface, the haptic glove should be user-friendly and effectively apply force to the fingers. A “user-friendly” glove is ergonomic and lightweight with a compact design that does not harm fingers. An “effective” glove provides controllable contact forces ranging from a gentle touch to full opposition to finger movement without kinematic constraints on the finger movement.

However, existing haptic gloves do not fully meet these criteria (i.e., user-friendly and effective) without shortcomings. Although significant research has been performed into haptic glove design [4–7,9–15], they either restrict the natural motion and maximum output force of the hand or are bulky and heavy.

Turner et al. [12] evaluated the CyberGrasp, a commercial haptic glove. The CyberGrasp is a haptic device with one-direction

(extension only) active force feedback on each finger [13]. The glove joints are actuated by a cable-driven mechanism that transmits the force loading from an actuation unit to each finger. The heavy actuation unit is located on the table or worn as a backpack. The maximum output force at each finger is 12 N and the entire device's workspace is a sphere of 1 m radius due to the limit of the cable length. The mass of the mechanism which must be worn on the hand is 539 g, and this can lead to user fatigue. Two key drawbacks of this system are its complexity and its cost (approximately \$39,000). In addition, the one-direction actuation mechanism only allows forces to be applied to the fingertips in the direction of extension, which limits its utility in force assistance grasp or rehabilitation application.

Some other haptic gloves utilize internal grasp structures [14–16]. Bouzit et al. [15] presented the Rutgers Master II, an active glove for dexterous virtual interactions and rehabilitation. The system is actuated by four pneumatic actuators arranged inside the palm of the hand. Hall effect sensors and infrared sensors are integrated with the actuation cylinders to reduce the necessity of a separate sensing glove. The objective of the mechanism is to deliver a compact and lightweight structure on the hand. The Rutgers Master II weighs 185 g including the wires and pneumatic tubing (excluding the pneumatic pump, power source, etc.), and provided forces up to 16 N on each of the four fingers. However, the Rutgers Master II limits the hand's workspace and prevents complete fist closure due to the placement of the actuators in the palm.

Based on the above analysis, the primary performance requirements of a new haptic glove design are detailed below:

- Size – The glove should easily fit on a human hand.
- Weight – The glove should be as light as possible for portability on a hand. To help achieve this goal, each finger should require only one dedicated actuator.
- Flexibility of Mechanism – The glove should match the hand's dexterity without limiting the hand's range of motion.
- Dynamic Range – The glove should be sufficiently versatile to be used in both highly sensitive and large force tasks.
- Safety – The user should be protected from any type of harm from the mechanism including protections built into the software and mechanical limits in the mechanism.

The glove mechanism presented in this work was designed to address these challenges. Figure 1 shows different configurations of one left hand wearing the glove in different views. This

Contributed by the Mechanisms and Robotics Committee of ASME for publication in the JOURNAL OF MECHANISMS AND ROBOTICS. Manuscript received November 24, 2013; final manuscript received December 12, 2014; published online March 23, 2015. Assoc. Editor: Pierre M. Laroche.

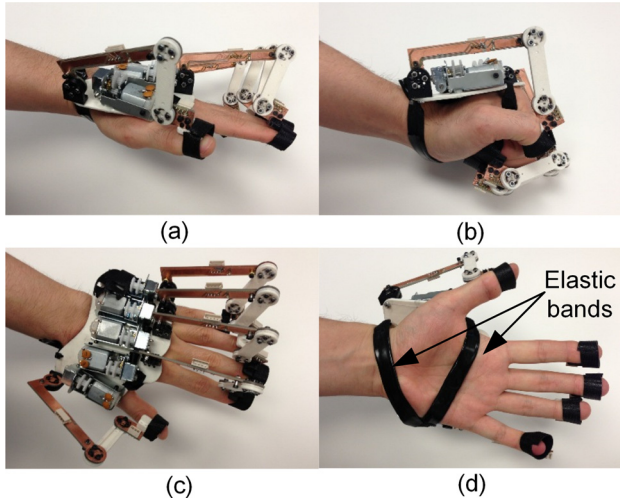


**Fig. 1** Glove prototype: (a) and (b) side view in open/closed configuration, (c) and (d) top/bottom view in open configuration

five-finger haptic interface represents a follow-up to the two-finger glove developed earlier [17]. The new glove is wireless, lightweight, easy, and comfortable to wear and operate. In addition to the extension to a five-finger design, with the optimization analysis, the new glove's workspace is increased by over 30%, and thus could adapt to larger range of different hand sizes and improved the transmission efficiency.

The main contributions of this paper are the mechatronic design and the optimization of a haptic glove mechanism. The paper is organized as follows: Section 2 describes the mechanical design of the system. Section 3 describes the numerical model of the mechanism and the optimization of the glove's finger segment lengths. Section 4 provides the simulation results and experimental validation of the mechanics model and control system, and Sec. 5 summarizes the paper and describes future work.

## 2 Glove Mechanism Design

**2.1 Mechanical Design.** The glove mechanism is composed of three basic elements: a support pad, five actuation units and five-finger mechanisms, as shown in Fig. 2. Table 1 lists the mass of each component of the glove (total mass is 310 g).

The support pad is custom-made of thermoplastic material in a curved shape to match the shape of the user's hand and rest on it comfortably. Two adjustable elastic bands are routed around the thumb and attach to the sides of the support pad, making the pad sit on the back of the user's hand tightly (Fig. 1(d)). The

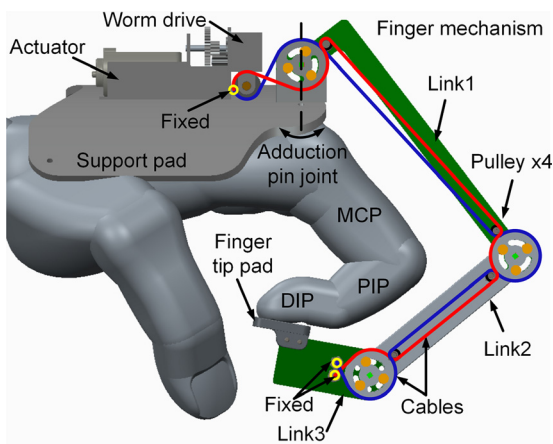


**Fig. 2** CAD model of the index finger mechanism of the glove

**Table 1** The glove component mass

| Component                   | Mass (g)      |
|-----------------------------|---------------|
| Support pad                 | 15            |
| Finger actuator $\times 5$  | $35 \times 5$ |
| Finger mechanism $\times 5$ | $15 \times 5$ |
| Control unit                | 25            |
| 9 V rechargeable battery    | 20            |
| Total mass                  | 310           |

adjustable elastic band allows the support pad to fit on different hand sizes easily. The support pad is used as the "ground" link of the finger mechanisms, and the actuators and electronics, including the battery, are all attached to the support pad.

Each finger mechanism is attached to the support pad through a passive pin joint which enables the finger to move in adduction and abduction directions freely. This mechanism has a mechanical limit which prevents the finger from rotating until it reaches a certain controlled position (approximately 5 deg in adduction/abduction direction). This 5 deg angle works fine for the four fingers, but it limits the thumb function due to the flexibility of the thumb, and this is one slight weakness of the current design). Each finger consists of three phalanges with interconnecting rotation joints, as shown in Fig. 2. This configuration follows the model of human physiology and imitates basic human hand characteristics. The fingertip pad, which is attached to link 3, attaches directly to the fingertip using an adjustable length Velcro wrap and applies both flexion and extension tendon forces (measured by strain gauge attached to the fingertip pad) directly to the finger. Because of this band, the glove can be put on quickly and is easily adjustable to different finger sizes. A thin, soft layer of fabric is wrapped around the inside of the Velcro band to make the glove comfortable to wear. As shown in Figs. 1 and 2, printed circuit board (PCB) is used to construct the mechanical links (link 1 and link 3) and to carry the electrical components (Hall Effect sensors to measure joint angles). This dual use allows the glove to be both lighter and stronger [17].

Based on the performance requirements in Sec. 1, the force feedback for each finger will be driven by a distinct actuation module. This requires the movements of the three joints of each finger—namely, the distal interphalangeal (DIP), the metacarpophalangeal (MCP), and the proximal interphalangeal (PIP) joints—to be accounted for in mapping the applied actuation command to the applied force at the fingertip. Each finger is controlled by an antagonistic pair of tendons which are routed along the finger exoskeleton to the fingertip through primary and secondary pulleys. These pulleys allow the motor to generate torques in each of the mechanism's joints. One end of each tendon is wound about the active pulley attached to the actuation module, while the other end is attached to the tip of Link 3. Figure 2 provides a side view of the active tendon assembly routed along to a glove finger. The pair of tendons is wound in opposite directions around the actuator spool to enable the tendons to transmit forces for both pulley rotation directions. These forces along the exoskeleton drive the links to follow or resist finger movement. In this antagonistic configuration, the actuator controls the relative length of the tendon pair, shortening one of the tendons while simultaneously lengthening the other. As shown in Fig. 2, when the actuator rotates the active pulley counterclockwise, the grasp tendon (red) is tensioned, and the mechanism/finger closes. When the active pulley rotates clockwise, the release tendon (blue) is tensioned and the mechanism/finger opens. The glove links allow full flexion and extension of all joints, and this tendon-driven mechanism does not have any limits in the adduction or abduction directions since this motion will not change the cable length. The material Dyneema was chosen for the tendon cabling because of its high strength and flexibility with minimal stretching and weight.

With a single motor driving three joints, each finger mechanism is under actuated. However, the motion of the glove is not directly

controlled by the motor; rather, the mechanism's motion is driven by the user's finger movement. The contact force between the user's fingers and the glove is what is regulated by the actuator.

**2.2 Worm Drive Mechanism.** In haptics applications, the contact force  $F$  is typically calculated as a linear function of the slave's virtual penetration distance  $x$  into the object and the slave's velocity ( $\dot{x}$ ) [1]. This results in a virtual spring-damper model for  $F$ , defined in Eq. (1), where  $k$  is the virtual object's stiffness and  $b$  is the object's damping coefficient

$$F = b\dot{x} + kx \quad (1)$$

A key challenge in haptics that has been repeatedly highlighted in the literature [12,16–19] is the difficulty in virtually representing very rigid or hard objects due to the limited stiffness of the haptic device. Even a solid block will seem to have some compliance to the touch. However, if  $k$  and  $b$  are set too high, undesirable oscillations often occur, and the touch sensation is unnatural to the operator [20].

In general, a haptic glove with force-feedback should be capable of delivering a maximum force that matches the human hand output force. According to Ref. [21], the maximum thumb/finger strength is 35 N (male sustained hold). The glove mechanism is able to provide this force due to the nonback drivable worm drive incorporated into the actuation module. Each actuator unit consists of a brushed DC-motor (Mabuchi FA-130, with a Tamiya 70103 universal gearbox at 101:1 gear ratio). The last stage of the gearing is a nonback drivable metal worm drive, with the active pulley (which actuates the finger mechanism) attached to the worm-gear shaft. This actuator is self-locking without power consumption, making the passive force as high as 35 N. The maximum active output force that the glove mechanism can provide on the fingertip is 10 N, which is slightly smaller than the 12 N maximum dynamic output force provided by CyberGrasp [13]. However, the 10 N is sufficient to provide realistic active force feedback and will not harm the operator's finger.

The benefit of the nonback drivable mechanism is seen when the haptic device is used to touch or feel some hard object (e.g., a concrete wall). In this situation, back drivable motor-actuated haptic devices would run the motor while stalled to generate the high force. Due to the current and power limits of haptic devices, the force resulting from this stall torque is still insufficient [22] compared to the human finger output force (35 N). However, for the glove mechanism in this situation, the motor current is zero by virtue of the self-locking characteristic of the worm-gear mechanism. Because such high force feedback only occurs in passive force output mode, it will not hurt the user's finger. With closed-loop force-feedback control, the glove can provide a realistic feeling of both hard and soft materials ranging from a concrete wall to soft cotton.

When the glove is powered on, with proper speed command to each actuator unit, it can provide force feedback proportional to the velocity difference between the finger's motion and that of the worm-gear mechanism. When the glove is powered off, each worm-gear mechanism becomes nonback drivable. Another benefit of the worm drive mechanism is that the power consumption of the actuators is very low. The 9 V battery can last as long as 40 min for continuous use of the entire glove.

### 3 Optimization of Link Length

In order to optimize the glove mechanism design presented in Sec. 2, a 4-bar finger mechanism with bidirectional tendon actuation is modeled and optimized relative to several composite design indexes simultaneously, including workspace size, force transmission ratio, and mechanical design parameters. Constrained optimality theory is applied to obtain the optimal sets of

link lengths. Glove-link-configurations optimized for special performance indices are also illustrated.

**3.1 Introduction.** For each finger, the haptic mechanism and the finger itself can be modeled as a single six-bar mechanism, as shown in Fig. 3, where the hand/support pad represents the ground. Each finger has three links, and the haptic mechanism for each finger has three links, too. However, the terminal link of each finger is assumed to be rigidly connected to the terminal link of the haptic mechanism through the Velcro strap discussed in Sec. 2. Therefore, there are 6 links in total (1 ground link, 3 finger links, 2 haptic mechanism links) and 6 revolute pin connections (ignoring the adduction/abduction due to its relative small range). According to Grubler's formula, the mobility of the system can be calculated using Eq. (2), where DF is the system's degrees of freedom (DOF),  $n = 6$  is the number of links,  $f_1 = 6$  is the number of lower-pair (1DOF) joints, and  $f_2 = 0$  is the number of higher-pair (2DOF) joints. Therefore, there are 3DOF in the system.

$$DF = 3(n - 1) - 2f_1 - f_2 = 3 \quad (2)$$

Based on Fig. 3, equations for the fingertip position ( $x_{A3}, y_{A3}$ ) and angle  $\phi$  are derived in Eqs. (3)–(5) in terms of the finger joint angles ( $\theta_1, \theta_2, \theta_3$ ) and the mechanism joint angles ( $\alpha_1, \alpha_2, \alpha_3$ ), where  $l_i$  is the length of the  $i$ th mechanism link  $\overline{B_{i-1}B_i}$ ,  $p_i$  is the length of the  $i$ th finger link  $\overline{A_{i-1}A_i}$ ,  $l_p$  is the length of  $\overline{B_3A_3}$ . In addition,  $s$  and  $c$  represent sine and cosine, functions such that  $c_{\alpha_1,12}$  is  $\cos(\alpha_1 + \alpha_2)$

$$\begin{aligned} x_{A3} &= x_{B_0} + l_1 c_{\alpha_1} + l_2 c_{\alpha_1,12} + l_3 c_{\alpha_1,123} + l_p c_{(90+\alpha_1,123)} \\ &= p_1 c_{\theta_1} + p_2 c_{\theta_1,12} + p_3 c_{\theta_1,123} \end{aligned} \quad (3)$$

$$\begin{aligned} y_{A3} &= y_{B_0} + l_1 s_{\alpha_1} + l_2 s_{\alpha_1,12} + l_3 s_{\alpha_1,123} + l_p s_{(90+\alpha_1,123)} \\ &= p_1 s_{\theta_1} + p_2 s_{\theta_1,12} + p_3 s_{\theta_1,123} \end{aligned} \quad (4)$$

$$\phi = \alpha_1 + \alpha_2 + \alpha_3 = \theta_1 + \theta_2 + \theta_3 \quad (5)$$

After solving Eqs. (3)–(5) according to Ref. [23], the mechanism joint angles  $\alpha_1, \alpha_2$ , and  $\alpha_3$  may be calculated using Eqs.

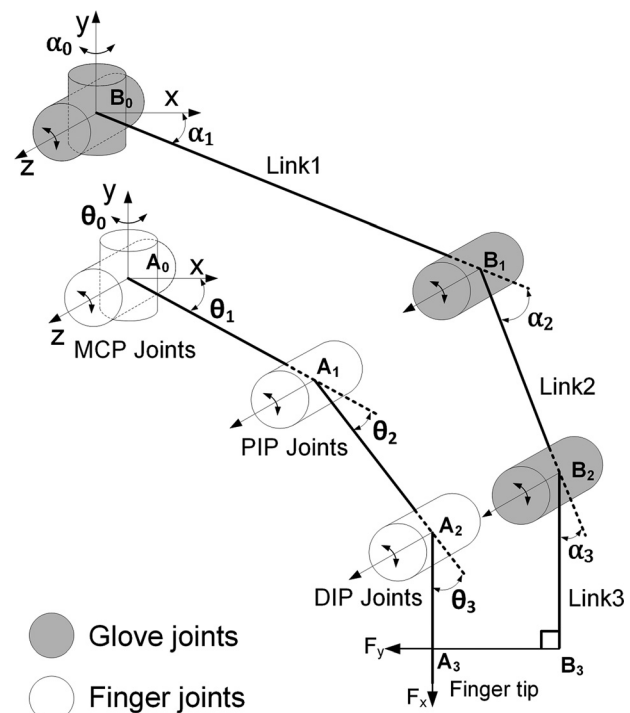


Fig. 3 Kinematic diagram of the finger/glove system

(6)–(8). Since the glove linkage is longer than the human finger, two solutions can be found: elbow up and elbow down configurations. In order to avoid the collision between the finger and the glove linkage, the elbow up solution is chosen. The finger angles  $\theta_1, \theta_2$ , and  $\theta_3$  are prescribed by the user

$$\alpha_1 = A \tan 2 \left( \frac{N}{M} \right) + \arccos \left( \frac{p_1^2 + p_2^2 + N^2 - M^2}{2p_1 \sqrt{M^2 + N^2}} \right) \quad (6)$$

$$\alpha_2 = \arccos \left( \frac{M^2 + N^2 - p_1^2 - p_2^2}{2p_1 p_2} \right) \quad (7)$$

$$\alpha_3 = \theta_1 + \theta_2 + \theta_3 - \alpha_1 - \alpha_2 \quad (8)$$

where

$$M = -x_{B_0} + l_1 c_{\theta_1} + l_2 c_{\theta_2} + (l_3 - p_3) c_{\theta_3} + l_p s_{\theta_2}$$

$$N = -y_{B_0} + l_1 s_{\theta_1} + l_2 s_{\theta_2} + (l_3 - p_3) s_{\theta_3} + l_p c_{\theta_2}$$

Next, the Jacobians of the mechanism are calculated. For this model, there will be two Jacobians  $J_q^u$  to relate the joint angular rates  $\dot{\mathbf{q}} = \{\dot{\theta}_i, \dot{\alpha}_i\}$  to the fingertip velocities  $\dot{\mathbf{u}}$ , as shown in Eq. (9): finger Jacobian  $J_\theta^u$  and mechanism Jacobian  $J_\alpha^u$

$$\dot{\mathbf{u}} = [\dot{x}_{A_3}, \dot{y}_{A_3}, \dot{\phi}]^T = J_q \dot{\mathbf{q}} \quad (9)$$

Here,  $J_q^u = [\partial \mathbf{u} / \partial q_1, \partial \mathbf{u} / \partial q_2, \partial \mathbf{u} / \partial q_3]$  is the Jacobian relating the task space coordinates  $\mathbf{u}$  to the joint space coordinates,  $\mathbf{q}$ . Based on this definition, the two Jacobians—finger  $J_\theta^u$  and mechanism  $J_\alpha^u$ —are defined by

$$J_\theta^u = \begin{bmatrix} b_{11} & b_{12} & b_{13} \\ b_{21} & b_{22} & b_{23} \\ 1 & 1 & 1 \end{bmatrix} \quad \text{and} \quad J_\alpha^u = \begin{bmatrix} a_{11} & a_{12} & a_{13} \\ a_{21} & a_{22} & a_{23} \\ 1 & 1 & 1 \end{bmatrix}$$

where  $b_{11} = -p_1 s_{\theta_1} - p_2 s_{\theta_2} - p_3 s_{\theta_3}$ ,  $b_{12} = -p_2 s_{\theta_2} - p_3 s_{\theta_3}$ ,  $b_{13} = -p_3 s_{\theta_3}$ ,  $b_{21} = p_1 c_{\theta_1} + p_2 c_{\theta_2} + p_3 c_{\theta_3}$ ,  $b_{22} = p_2 c_{\theta_2} + p_3 c_{\theta_3}$ ,  $b_{23} = p_3 c_{\theta_3}$ ,  $a_{11} = -l_1 s_{\alpha_1} - l_2 s_{\alpha_2} - l_3 s_{\alpha_3} - l_p c_{\alpha_1}$ ,  $a_{12} = -l_2 s_{\alpha_2} - l_3 s_{\alpha_3} - l_p c_{\alpha_2}$ ,  $a_{13} = -l_3 s_{\alpha_3} - l_p c_{\alpha_3}$ ,  $a_{21} = l_1 c_{\alpha_1} + l_2 c_{\alpha_2} + l_3 c_{\alpha_3} - l_p s_{\alpha_1}$ , and  $a_{22} = l_2 c_{\alpha_2} + l_3 c_{\alpha_3} - l_p s_{\alpha_2}$ ,  $a_{23} = l_3 c_{\alpha_3} - l_p s_{\alpha_3}$ .

Since this finger–glove system has 3DOF, three joint angles must be specified to define the configuration. If the three human finger joints (MCP, DIP, and PIP) are selected as input angles, the finger–glove mechanism can be considered dependent, or vice versa. Therefore, the internal kinematic relationship between dependent joints and independent joints is required to deal with the problem mentioned above.

The equivalent velocity relation is given by

$$\dot{\mathbf{u}} = J_\theta^u \dot{\boldsymbol{\theta}} = J_\alpha^u \dot{\boldsymbol{\alpha}} \quad (10)$$

where  $\dot{\boldsymbol{\theta}} = [\dot{\theta}_1, \dot{\theta}_2, \dot{\theta}_3]^T$  and  $\dot{\boldsymbol{\alpha}} = [\dot{\alpha}_1, \dot{\alpha}_2, \dot{\alpha}_3]^T$ .

Premultiplying the inverse of the matrix  $J_\theta^u$  to the second and third terms in Eq. (10) results in the following equation:

$$\dot{\boldsymbol{\theta}} = (J_\theta^u)^{-1} J_\alpha^u \dot{\boldsymbol{\alpha}} = J_\alpha^0 \dot{\boldsymbol{\alpha}} \quad (11)$$

where  $J_\alpha^0$  denotes the first order kinematic matrix relating  $\boldsymbol{\theta}$  to  $\boldsymbol{\alpha}$ .

According to the velocity/force duality [23], the force relation between the independent joints and the dependent joints can be defined using the following equation:

$$\boldsymbol{\tau}_\alpha = (J_\alpha^0)^T \boldsymbol{\tau}_\theta \quad (12)$$

**3.2 Geometric Optimization.** In haptics, a key requirement is that the human operator's movement should not be restricted by

the haptic device when there is no contact with a remote or virtual object. Thus, adequate DOF and sufficient workspace are required for the haptic device, especially for the haptic glove worn on the operator's hand, the most dexterous part of the human body.

The finger–glove's geometric parameters, particularly link length, determine the properties of the linkage such as its workspace and force transmission ratio. In this research, the link lengths are optimized to be able to enhance the glove's workspace, and maximize the force transmission ratio and avoid collision between each finger and the glove mechanism. Thus, the problem is formulated as a multi-objective optimization function that optimizes over the force transmission ratio and contact force magnitude subject to geometric, and collision avoidance constraints. The design variables to be optimized are the link lengths  $l_1, l_2$ , and  $l_3$ , as shown in Fig. 3.

Furthermore, in order to increase the collision free workspace, the first link of the glove is composed of two perpendicular segments, resulting in an L shape as illustrated in Fig. 2.

**3.3 Force Transmission Ratio Objective Function.** The values of the link lengths are a function of the size of a human finger and the finger joint angular motion ranges. However, these properties vary across the human population quite significantly. To avoid the need to customize a glove for each unique user, it is desirable to accommodate a large number of different users with a given design. From Eqs. (3)–(5), the conclusion can be drawn that the solutions always exist if the finger length is much shorter than the total length of the mechanism (about 140 mm), thus the glove mechanism design can accommodate variations in finger length. Figure 1 demonstrates that the same mechanism can easily adapt to different finger sizes because each articulated linkage mechanism remains extendable when each finger is fully stretched.

In order to accommodate a wide variety of users, the “stochastic reachable workspace” method was adopted into the design of the glove interface mechanisms [24]. The workspace and average dimensions of a male index finger are shown in Table 2 [25].

According to the inverse kinematic analysis in Sec. 3.1, given a set of link lengths  $l_i$ , the mechanism joint angles  $\alpha_i$  can be calculated given the finger joint angles  $\theta_i$  if solutions exist according to Eqs. (3)–(5). Thus, Eq. (13) summarizes the relation mentioned above

$$\alpha_i = f(\theta_i, l_i) \quad (13)$$

Joint range is defined as

$$\alpha_{i,\text{var}} = \alpha_{i,\text{max}} - \alpha_{i,\text{min}}, \quad i \in \{1, 2, 3\} \quad (14)$$

Each finger of the glove mechanism is actuated by a motor rotation that generates tension in a pair of tendons. The tendons are routed from the actuator through pulleys to the fingertip. However, friction between the tendons and the pulleys reduces the amount of force available to the finger tip. To compensate this, the actuator must generate more tension, which may result in low efficiency, high current, and, eventually, damage to the motor or the mechanism. Therefore, the efficiency issues in cable and pulley systems must be thoroughly understood. Some relevant research on friction efficiency has been described in Refs. [26] and [27]. However, understanding the tendon friction

**Table 2 Normal values for range of motion of joints**

| Finger joint | Angular motion range (deg) | Finger link length (mm) |
|--------------|----------------------------|-------------------------|
| MCP          | [−90, 30]                  | 48.3                    |
| PIP          | [−120, 0]                  | 28.2                    |
| DIP          | [−80, 0]                   | 19.1                    |

characteristics in our particular application is not common and is therefore discussed and experimentally tested herein.

Nonlinear complex friction phenomena are the main reasons for the inefficiencies and loss of tendon transmission. Coulomb friction, viscous friction, and static friction can all be present in tendon transmission systems [28]. To actuate the glove mechanism, the tendon needs to slide within the groove of the pulley. Therefore, only kinetic friction is considered in this paper.

If the tendon wraps around the pulley at a given angle  $\gamma$ , the ratio between tendon tension force before  $F_1$  and after  $F_2$  routing may be modeled using Eq. (15), where  $\mu$  is the coefficient of friction caused by sliding motion between the tendon and pulley [26].

$$F_1/F_2 = e^{\mu\gamma} \quad (15)$$

It is important to note that the pulley radius, magnitude of the cable tension, and sliding velocity do not influence the tendon friction. Because the glove mechanism tendon material (dyneema) is very soft, even a very small pulley radius will not accelerate cable wear, and the friction coefficient will not be affected over time. Therefore, the secondary pulleys are made of a 2 mm screw and a steel ring, as shown in Fig. 4, and the secondary pulley is modeled as a stationary cylinder.

As Eq. (15) indicates, the main parameters influencing cable transmission efficiency are  $\gamma$  and  $\mu$ . While  $\mu$  is dictated by the tendon and cylinder materials,  $\gamma$  depends on the mechanism geometry. As shown in Eq. (16),  $\gamma$  may be broken down into two components: a constant component  $\gamma_c$  corresponding to the minimum wrap angle configuration and a variable component  $\Delta\gamma$  that depends on the geometric configuration of the mechanism. The maximum value of  $\Delta\gamma$  for each joint is the joint range  $\alpha_{i,\text{var}}$ , defined in Eq. (14)

$$\gamma = \gamma_c + \Delta\gamma \quad (16)$$

In order to maximize the tendon force transmission ratio, the wrap angle for each joint should be minimized. This corresponds to minimizing the joint range  $\alpha_{i,\text{var}}$  at each joint. The norm of these angles is chosen to formulate the scalar force transmission ratio objective function  $z_1$ , as shown in the following equation:

$$z_1 = \sqrt{\alpha_{1,\text{var}}^2 + \alpha_{2,\text{var}}^2 + \alpha_{3,\text{var}}^2} \quad (17)$$

**3.4 Contact Force Objective Function.** The primary force that will be sensed by each finger in the glove mechanism will be the normal force applied to the surface of the fingertip [29,30]. The accuracy of the magnitude of this normal force  $f_y$ , as shown in Fig. 3, is a key factor in haptic glove and precision teleoperation grasping tasks applications. Thus, the contact force components in other directions ( $f_x$  and  $f_z$ ) are ignored.

The joint torques ( $\tau_1$ ,  $\tau_2$ , and  $\tau_3$ ) are calculable from the fingertip contact force  $\mathbf{F} = [f_x, f_y, f_z]^T$  and the mechanism Jacobian,  $J_x^\mu$  according to the following equation:

$$[\tau_1, \tau_2, \tau_3]^T = (J_x^\mu)^T [f_x, f_y, f_z]^T \quad (18)$$

After substituting for  $J_x^\mu$  and setting  $f_x$  and  $f_z$  to zero, the joint torques become  $\tau_1 = a_{21}f_y$ ,  $\tau_2 = a_{22}f_y$ , and  $\tau_3 = a_{23}f_y$ . To

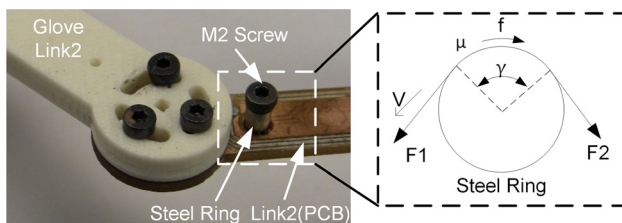


Fig. 4 Fixed secondary pulley prototype and model

maximize the contact forces for a given set of joint torques, these coefficients should be minimized. As before, the norm of these coefficients is chosen to formulate the scalar contact force objective function  $z_2$  as shown in the following equation:

$$z_2 = \sqrt{a_{21}^2 + a_{22}^2 + a_{23}^2} \quad (19)$$

**3.5 Constraints.** The multi-objective optimization problem is subject to constraints related to limitations in mechanical design, kinematic configurations and the collision-free operational requirement.

In order to fit on a human hand, the total length of each of the glove's fingers should be greater than the length of an average human finger. Therefore, kinematic constraint  $g_1$  ensures the total length of the mechanism is greater than the total length of the average finger segments, as defined in the following equation:

$$g_1 : l_1 + l_2 + l_3 > p_1 + p_2 + p_3 \quad (20)$$

In addition, the glove mechanism link 1 should exceed the finger segment 1 length to prevent the intersection between the finger and glove mechanism. Therefore, kinematic constraint  $g_2$  ensures link 1 length is greater than the length of the finger's first segment, as shown in the following equation:

$$g_2 : l_1 > p_1 \quad (21)$$

Due to mechanical design constraints, each joint of the glove finger cannot continuously rotate and its working range is limited to a maximum of 150 deg. This joint angle limit also protects the user's fingers from rotating beyond normal range of motion and causing injury. Therefore, kinematic constraint  $g_3$  will restrict the joint range  $\alpha_{i,\text{var}}$  at each joint  $i$  to less than 150 deg, as shown in the following equation:

$$g_3 : \alpha_{i,\text{var}} < 150 \text{ deg}, \quad i \in \{1, 2, 3\} \quad (22)$$

**3.6 Collision-Avoidance Constraint.** If the glove link lengths are not properly designed, intersection between the finger and glove mechanism will occur. In order to avoid this intersection, collision detection algorithms are incorporated into the optimization procedure. From Fig. 3, each pair of segments,  $B_{i-1}B_i$  and  $A_{i-1}A_i$  for  $i = 1, 2, 3$  are examined. When collision is detected, the associated mechanism joint angles are excluded from the optimal result, as shown in Fig. 5, where the solutions at which intersections occurred are marked in red.

**3.7 Optimization Formulation and Results.** Based on Eqs. (17) and (19), the multi-objective optimization function may be defined by Eq. (23), where  $w_1$  and  $w_2$  are the weighting coefficients, and is subject to the constraints defined in Eqs. (20)–(22)

$$Z = w_1 z_1 + w_2 z_2 \quad (23)$$

In order to solve this constrained nonlinear optimization, two methods are used. The second derivatives of the Lagrangian method using the brute-force global search (BFGS) formula at each iteration (implemented with MATLAB optimization toolbox using the *fmincon* function) was obtained to find the local minimum value of the penalty function. The BFGS method was also used to verify that the result was correct.

For the numerical optimization, a set of initial guesses (the lengths of human hand fingers from Table 2 multiplied by 1.5) and the lower (human fingers lengths from Table 2) and upper (fingers lengths from Table 2 multiplied by 2) boundaries were chosen and all of the weight coefficients were set to 1 (implying equal importance for all two objective functions).

The optimal length of link 3 quickly converges to 19.1 mm, so only link 1 and link 2 are shown in Fig. 5. The optimized solution

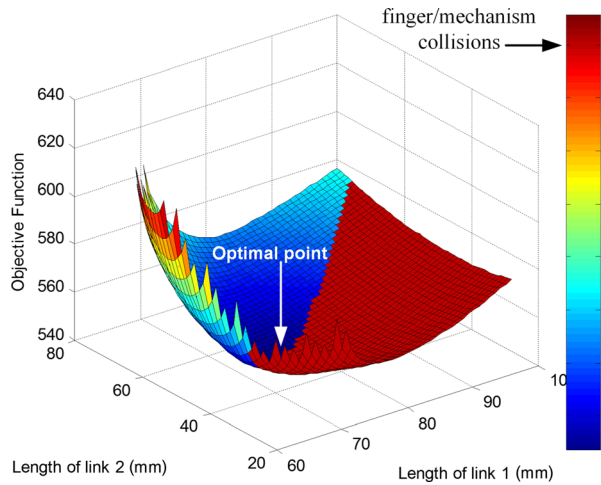


**Fig. 5 Optimal result (local minimum, variance (19, 18) = 543.6889)**

set, with minimum objective functions that satisfy all the constraints, was summarized in Table 3.

In order to find the singular points of the glove mechanism, the determinant of its Jacobian should be set equal to zero, as shown in Eq. (24). A singularity will occur when  $\alpha_2$  equals zero or 180 deg. However, for the glove mechanism, the working range of  $\alpha_2$  is  $[-130, -50]$ , which will avoid all calculated singularities

$$\det(J_{\alpha}^u) = l_1 l_2 \sin \alpha_2 = 0 \quad (24)$$

#### 4 Simulation and Experiments

**4.1 Index Finger Workspace Simulation.** Two methods are used to calculate the workspace of the human finger and the glove mechanism: joint angle sweep and the recursive swept boundary method. For the joint angle sweep, large numbers of points are generated in the workspace based on varying the joint angles through their known ranges, and the workspace boundary is computed based on these points. Whereas this method is computationally inefficient, it is relatively simple to implement and highly accurate. Alternatively, the recursive swept boundary method [31] is very computationally efficient. However, it is significantly more difficult to implement.

Based on the mechanism model defined in Sec. 2, the finger joint ranges of motion defined in Table 2, and the optimal link lengths calculated in Sec. 3.7, the 2D workspace for a finger and the glove mechanism can be obtained, as shown in Fig. 6. As the figure illustrates, the finger workspace is a subset of the mechanism's workspace, ensuring the glove allows unimpeded finger motion. Similar results are seen for the workspaces of the other fingers and mechanisms.

**4.2 Friction Model Validation.** Figure 7 shows the apparatus used to measure the friction coefficient between the tendon and stationary pulley. A custom manufactured plate was designed to ensure that the wrap angles were at specific desired values. To experimentally simulate the tension over the stationary pulley, a weight was suspended from one end of the tendon. In addition, to prevent static friction effects, a 50 W brushless motor with a 23:1

**Table 3 Optimization results of the glove link**

| Glove link/joint | Joint angle range (deg) | Link length (mm) |
|------------------|-------------------------|------------------|
| 1                | $[-79.86, 59.98]$       | 73.88            |
| 2                | $[-127.8, -58.3]$       | 47.23            |
| 3                | $[-82.3, 81.6]$         | 19.1             |

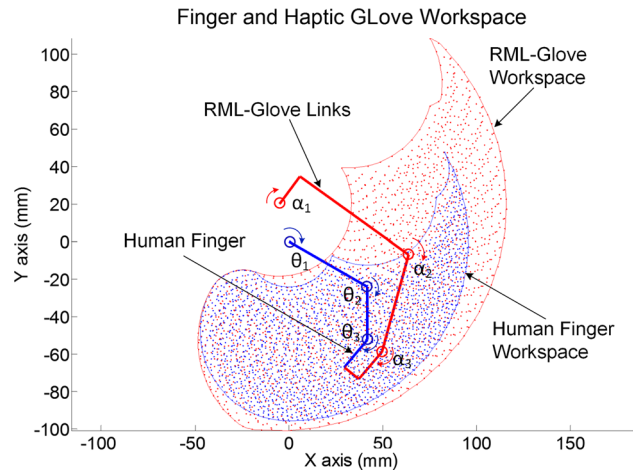


**Fig. 6 2D workspace comparison between index finger and the glove mechanism when  $l = [73.88; 47.23; 19.1]$ ,  $\alpha_1 = [-80, 60]$ ,  $\alpha_2 = [-130, -50]$ ,  $\alpha_3 = [-80, 60]$**

planetary gearbox (Maxon Gear 166936, Maxon Motor 251601) was attached to the tendon spool, lifting and lowering the weight at various constant speeds. A load cell (MLP-10, Transducer Techniques, Inc.) was connected in series with the tendon between the active tendon spool (connected to the motor) and the stationary pulley to measure the tension of the tendon. In addition, different lubrication conditions were tested to evaluate the lubricant's effect on the friction coefficient.

The wrap angle was varied from 45 to 315 deg in 45 deg increments to evaluate its effect on the friction coefficient, and the mass at the end of the tendon was varied from 100 g to 1000 g in 100 g increments. When the actuator lifts the weight, the load cell measures the active pulling force  $F_1$  in Eq. (15), and the hanging weight corresponds to  $F_2$ . Conversely, when the actuator lowers the weight, the load cell measures  $F_2$  and the weight is  $F_1$ .

The linear behavior of the experimental results shown in Fig. 8 and the close friction coefficient values when the wrap angles vary as shown in Fig. 9 suggest that Eq. (15) is an acceptable model of the tension system when the wrap angle is above 90 deg, which will always be satisfied for the glove mechanism. The effective friction coefficient can be found by applying a least-squares fitting to the data for 90 deg wrap and above. The average friction coefficients for lubricated  $\mu_L$  and nonlubricated  $\mu_{NL}$  conditions are 0.0530 and 0.0631, respectively.

**4.3 Free Movement Test.** The capability of free motion is a basic evaluation criterion of haptic devices [32,33]. In the free

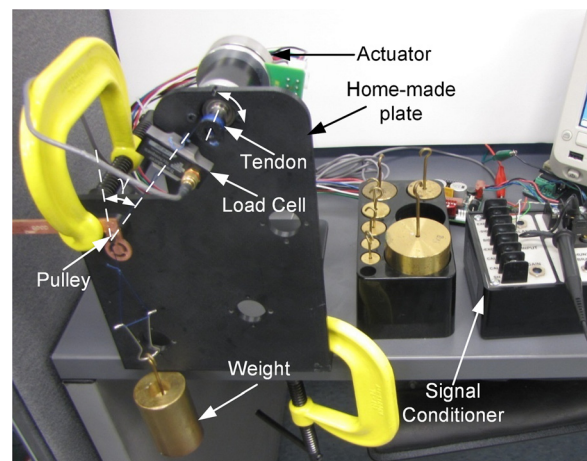


**Fig. 7 Friction model validation experimental test platform**

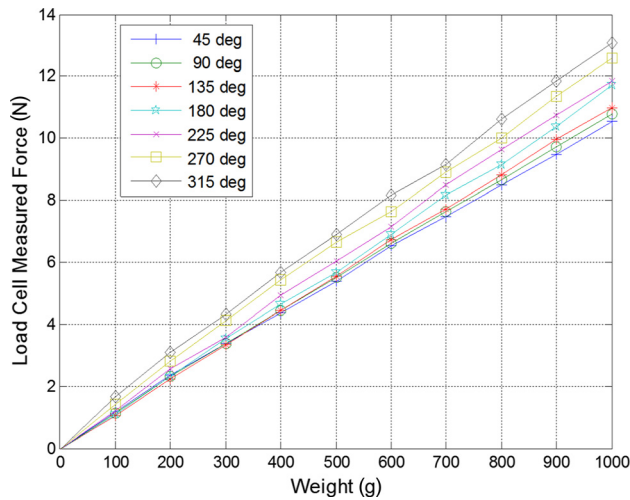


**Fig. 8** Least-squares fitting plots for load cell output when lifting objects with lubrication

motion mode (i.e., the state with zero force input), the haptic glove's user should be able to move his/her fingers freely without feeling resistance or inertia from the glove. The resistance and inertia should be compensated for via a real-time control algorithm based on the force and position sensors input. It is assumed that the force between the glove and the human finger should be as small as possible in free motion. If we control the device and set the force to be zero, the glove will follow the movement of the user's fingers. Thus, the user cannot feel the resistance force.

In this experiment, 4 male and 1 female subjects were asked to wear the glove prototype and to move all fingers in close/open maneuvers, in two different modes: without cabling and with cabling. In the "without cabling" mode, all the actuation cables were removed. Without the worm-gear locking function, the finger mechanisms move easily even under a small external force. To test whether the glove is comfortable to wear, 25 people were asked to perform the wear test (repeat fully open/close maneuvers three times) in this mode. None has reported any hand movement constraint issues. The "with cabling" mode is the normal glove mechanism system with the cable installed and force feedback enabled. In this second mode, the control algorithm actively positions the actuators to ensure the glove mechanism tracks the finger's movement.

The glove does not require calibration for different users. However, before the test, the finger length of each user was measured by a ruler. During the test, each user was asked to repeat two close-open hand maneuvers five times in approximately 3 s in both modes. The 15 joint angle sensors of the glove measured the joints angles at a sampling frequency of 300 Hz. Before recording the data, each user spent several minutes to get used to the system.

The graphical results for two close/open maneuvers acquired by the first user's index finger in test no. 1 are reported in this paper

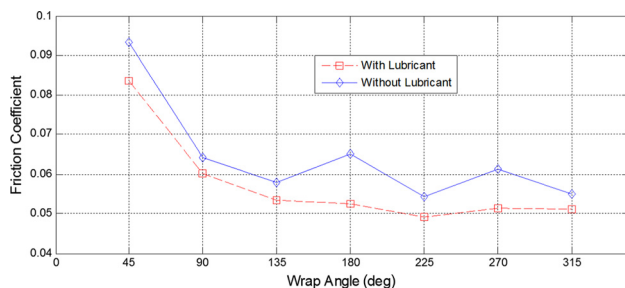


**Fig. 9** Friction coefficient with and without lubrication

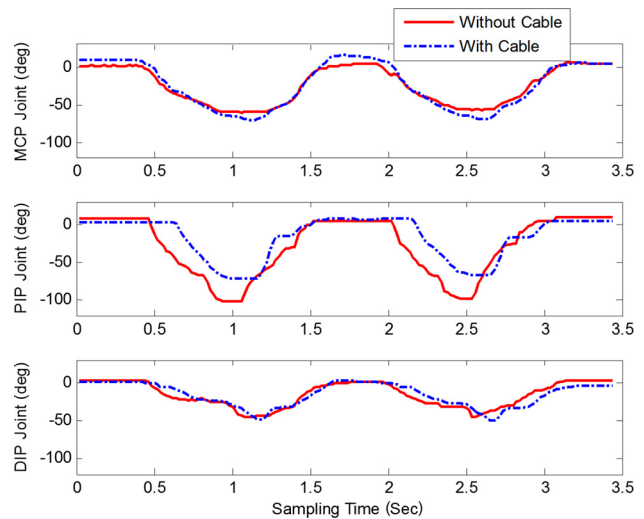


**Fig. 10** Human index finger trajectories for two close/open maneuvers acquired by user 1 in test #1

as a representative example of the total test results. Five parameters are displayed for the two modes in Figs. 10 and 11: the three measured joint angle trajectories, the contact force and the actuator current (note that the actuator current is not applicable to the "without cabling" mode because the motor is not used). In each test, the user took about 1 s for one full close/open maneuver. The glove can be actuated faster, but for safety considerations the maximum speed was limited to 1 s for one full close/open maneuver. At this speed, the maximum contact forces were approximately 200 mN in the "without cable" mode and 100 mN in the "with cable" mode. This result shows that the mechanism's internal resistance can be effectively compensated by a proportional integral derivative (PID) force controller. Since the main focus of this paper is the five-finger glove design and optimization, details on the control algorithm can be found in Ref. [17].

Pearson product moment correlation ( $r_p$ ) [34] was adopted to assess the level of similarity of joint trajectories between two different modes. Table 4 records the values of  $r_p$  and the standard deviation (s.d.) averaged over the five repetitions. As shown in Table 4, the slight differences between two different modes demonstrate the effectiveness of the haptic glove in following the movement of the user's fingers.

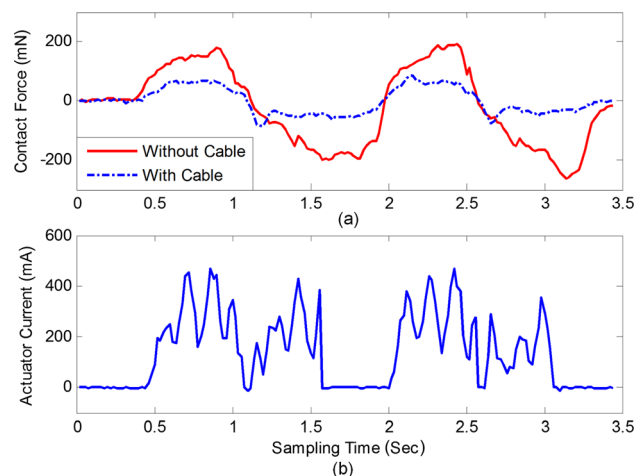


**Fig. 11** Contact force (a) and actuator current (b) measured in free movement

**Table 4 Product moment correlation**

|                          | User 1              | User 2              | User 3              | User 4              | User 5              | All uses            |
|--------------------------|---------------------|---------------------|---------------------|---------------------|---------------------|---------------------|
| $r_p(\alpha_1) \pm s.d.$ | 0.9907 $\pm$ 0.0022 | 0.9923 $\pm$ 0.0037 | 0.8671 $\pm$ 0.0542 | 0.9722 $\pm$ 0.0144 | 0.8864 $\pm$ 0.0842 | 0.9417 $\pm$ 0.0602 |
| $r_p(\alpha_2) \pm s.d.$ | 0.9135 $\pm$ 0.0227 | 0.7635 $\pm$ 0.0314 | 0.7163 $\pm$ 0.1012 | 0.8702 $\pm$ 0.0867 | 0.8034 $\pm$ 0.0770 | 0.7981 $\pm$ 0.0814 |
| $r_p(\alpha_3) \pm s.d.$ | 0.8992 $\pm$ 0.0471 | 0.9018 $\pm$ 0.0126 | 0.8134 $\pm$ 0.0261 | 0.9139 $\pm$ 0.0408 | 0.7413 $\pm$ 0.0865 | 0.8692 $\pm$ 0.0558 |

**5 Conclusions and Future Work**

The main contributions of this paper are: (1) the mechatronic design of a haptic glove mechanism, (2) the optimization of the mechanism’s geometry based on geometric and force transmission characteristics. Primarily, we proposed a method to optimize the link length in a haptic glove design for the purpose of enhancing the workspace of the mechanism and maximizing the force transmission ratio of the link mechanism. Free motion experiments were established to demonstrate the effectiveness of resistance compensation. The research has shown that a lightweight compact actuation package can provide excellent motion and force control potential in a complex, dexterous manipulator.

Future work will be devoted to the redesign of the thumb mechanism in order to add one more DOF to adopt the flexibility of the thumb joint. Furthermore, dynamic constraints optimization, such as the unintended force between the finger and the glove due to the non-back drivable actuator, will be addressed. For virtual reality applications, object recognition experiments will be conducted. For rehabilitation application, this system will be exploited to record and analyze the common movements of hand function including grip and release patterns, thus the glove could generate these movement patterns in playback fashion to assist a weakened hand to accomplish these movements, or to modulate the assistive level based on the user’s intent for the purpose of hand rehabilitation therapy. For virtual reality applications, “Digital Clay”, a three-dimensional haptic computer interface [35] will be used to interact with the five-finger glove to evaluate the glove design and functionality. For tele-operation applications, the glove mechanism will be adapted for hand gesture-based remote control of mobile robots [36–38].

**References**

[1] Khatib, O., and Siciliano, B., 2008, *Springer Handbook of Robotics*, Springer, Berlin, Germany.

[2] Bar-Cohen, Y., and Breazeal, C., 2003, *Biologically-Inspired Robots*, SPIE, Bellingham, WA, Vol. PM122.

[3] Burdea, G., and Coiffet, P., 2003, *Virtual Reality Technology*, Vol. 1, 2nd ed., Wiley, New York, p. 107.

[4] Jack, D., Boian, R., Merians, A. S., Tremaine, M., Burdea, G. C., Adamovich, S. V., Reece, M., and Poizner, H., 2001, “Virtual Reality-Enhanced Stroke Rehabilitation,” *IEEE Trans. Neural Syst. Rehabil. Eng.*, **9**(3), pp. 308–318.

[5] Fang, H., Xie, Z., and Liu, H., 2009, “An Exoskeleton Master Hand for Controlling DLR/HIT Hand,” *IEEE/RSJ International Conference on Intelligent Robots and Systems (IROS 2009)*, St. Louis, MO, Oct. 10–15, pp. 3703–3708.

[6] Luo, X., Kline, T., Fischer, H., Stubblefield, K., Kenyon, R., and Kamper, D., 2005, “Integration of Augmented Reality and Assistive Devices for Post-Stroke Hand Opening Rehabilitation,” *IEEE-EMBS 27th Annual International Conference of the Engineering in Medicine and Biology Society (IEEE-EMBS 2005)*, Shanghai, China, Sept. 1–4, pp. 6855–6858.

[7] Popescu, V. G., Burdea, G. C., Bouzit, M., and Hentz, V. R., 2000, “A Virtual-Reality-Based Telerehabilitation System With Force Feedback,” *IEEE Trans. Inf. Technol. Biomed.*, **4**(1), pp. 45–51.

[8] Massie, T. H., and Salisbury, J. K., 1994, “The PHANToM Haptic Interface: A Device for Probing Virtual Objects,” *ASME Winter Annual Meeting, Symposium on Haptic Interfaces for Virtual Environment and Teleoperator Systems*, Chicago, IL, Nov. 13–18, pp. 295–302.

[9] Tan, H. Z., Srinivasan, M. A., Eberman, B., and Cheng, B., 1994, “Human Factors for the Design of Force-Reflecting Haptic Interfaces,” *ASME Dyn. Syst. Control*, **55**(1), pp. 353–359.

[10] Ambrose, R. O., Aldridge, H., Askew, R. S., Burrigge, R. R., Bluethmann, W., Difter, M., Lovchik, C., Magruder, D., and Rehnmark, F., 2000, “Robonaut: NASA’s Space Humanoid,” *IEEE Intell. Syst.*, **15**(4), pp. 57–63.

[11] Bicchi, A., 2000, “Hands for Dexterous Manipulation and Robust Grasping: A Difficult Road Toward Simplicity,” *IEEE Trans. Rob. Autom.*, **16**(6), pp. 652–662.

[12] Turner, M., Gomez, D., Tremblay, M., and Cutkosky, M., 1998, “Preliminary Tests of an Arm-Grounded Haptic Feedback Device in Telemanipulation,” *Proc. ASME WAM, DSC-64*, pp. 145–149.

[13] VRLogic, 1999, “CyberGrasp,” VRLogic GmbH, Dieburg, Germany, <http://www.vrlogic.com/index.php/en/datagloves/cyberglovesystems>

[14] Kawasaki, H., and Mouri, T., 2007, “Design and Control of Five-Fingered Haptic Interface Opposite to Human Hand,” *IEEE Trans. Rob.*, **23**(5), pp. 909–918.

[15] Bouzit, M., Burdea, G., Popescu, G., and Boian, R., 2002, “The Rutgers Master II-New Design Force-Feedback Glove,” *IEEE/ASME Trans. Mechatron.*, **7**(2), pp. 256–263.

[16] Heuser, A., Kourtev, H., Winter, S., Fensterheim, D., Burdea, G., Hentz, V., and Forducey, P., 2007, “Telerehabilitation Using the Rutgers Master II Glove Following Carpal Tunnel Release Surgery: Proof-of-Concept,” *IEEE Trans. Neural Syst. Rehabil. Eng.*, **15**(1), pp. 43–49.

[17] Ma, Z., and Ben-Tzvi, P., 2015, “RML Glove—An Exoskeleton Glove Mechanism With Haptics Feedback,” *IEEE/ASME Trans. Mechatron.*, **20**(2), pp. 641–652.

[18] Borghesan, G., Macchelli, A., and Melchiorri, C., 2010, “Interconnection and Simulation Issues in Haptics,” *IEEE Trans. Haptics*, **3**(4), pp. 266–279.

[19] Shen, X., and Goldfarb, M., 2006, “On the Enhanced Passivity of Pneumatically Actuated Impedance-Type Haptic Interfaces,” *IEEE Trans. Rob.*, **22**(3), pp. 470–480.

[20] Kuchenbecker, K. J., Fiene, J., and Niemeyer, G., 2006, “Improving Contact Realism Through Event-Based Haptic Feedback,” *IEEE Trans. Visual. Comput. Graphics*, **12**(2), pp. 219–230.

[21] NASA, 2008, “Arm, Hand, and Thumb/Finger Strength,” Figure 4, National Aeronautics and Space Administration, Washington, DC, <http://msis.jsc.nasa.gov/sections/section04.htm#Figure%204.9.3-4>

[22] Heo, P., Gu, G. M., Lee, S., Rhee, K., and Kim, J., 2012, “Current Hand Exoskeleton Technologies for Rehabilitation and Assistive Engineering,” *Int. J. Precis. Eng. Manuf.*, **13**(5), pp. 807–824.

[23] Craig, J. J., 1989, *Introduction to Robotics*, 2nd ed., Addison-Wesley Publishing Company, Reading, MA.

[24] Venema, S., and Hannaford, B., 2001, “A Probabilistic Representation of Human Workspace for Use in the Design of Human Interface Mechanisms,” *IEEE/ASME Trans. Mech.*, **6**(3), pp. 286–294.

[25] Merck, 2010, “Physical Therapy (PT),” Merck & Co., Inc., Whitehouse Station, NJ, [http://www.merckmanuals.com/professional/special\\_subjects/rehabilitation/physical\\_therapy\\_pt.html](http://www.merckmanuals.com/professional/special_subjects/rehabilitation/physical_therapy_pt.html)

[26] Carlson, L. B., Veatch, B. D., and Frey, D., 1995, “Efficiency of Prosthetic Cable and Housing,” *J. Prosthet. Orthot.*, **7**(3), pp. 96–99.

[27] Schiele, A., 2008, “Performance Difference of Bowden Cable Relocated and Non-Relocated Master Actuators in Virtual Environment Applications,” *IEEE/RSJ International Conference on Intelligent Robots and Systems (IROS 2008)*, Nice, France, Sept. 22–26, pp. 3507–3512.

[28] Schiele, A., Letier, P., Van Der Linde, R., and Van Der Helm, F., 2006, “Bowden Cable Actuator for Force Feedback Exoskeletons,” *IEEE/RSJ International Conference on Intelligent Robots and Systems (IROS 2006)*, Beijing, China, Oct. 9–15, pp. 3599–3604.

[29] Minsky, M., Ouh-young, M., Steele, O., Brooks, F., Jr., and Behensky, M., 1990, “Feeling and Seeing: Issues in Force Display,” *Comput. Graphics*, **24**(2), pp. 235–243.

[30] Springer, S., and Gadh, R., 1997, “Haptic Feedback for Virtual Reality Computer Aided Design”, *ASME International Mechanical Engineering Congress and Exposition*, Dallas, TX, Nov. 16–21.

[31] Korien, J. U., 1984, “A Geometric Investigation of Reach,” Ph.D., Department of Computer Science, University of Pennsylvania, Philadelphia, PA.

[32] Research Laboratory of Electronics, 1992, “RLE Progress Report No. 135,” Massachusetts Institute of Technology, Cambridge, MA, <http://www.dtic.mil/dtic/tr/fulltext/u2/a266730.pdf>, p. 305.

[33] Ohashi, T., Szemes, P., Korondi, P., and Hashimoto, H., 1999, “Nonlinear Disturbance Compensation for Haptic Device,” *IEEE International Symposium on Industrial Electronics (ISIE ’99)*, Bled, Slovenia, July 12–16, Vol. 1, pp. 304–309.

[34] Rodgers, J. L., and Nicewander, W. A., 1988, “Thirteen Ways to Look at the Correlation Coefficient,” *Am. Stat.*, **42**(1), pp. 59–66.

[35] Rossignac, J., Allen, M., Book, W. J., and Glezer, A., 2003, “Finger Sculpting With Digital Clay: 3D Shape Input and Output Through a Computer-Controlled Real Surface,” *Shape Modeling International*, Seoul, South Korea, May 12–15, pp. 229–231.

[36] Ben-Tzvi, P., Goldenberg, A. A., and Zu, J. W., 2008, “Design and Analysis of a Hybrid Mobile Robot Mechanism With Compounded Locomotion and Manipulation Capability,” *ASME J. Mech. Des.*, **130**(7), p. 072302.

[37] Ben-Tzvi, P., 2010, “Experimental Validation and Field Performance Metrics of a Hybrid Mobile Robot Mechanism,” *J. Field Rob.*, **27**(3), pp. 250–267.

[38] Ben-Tzvi, P., Goldenberg, A. A., and Zu, J. W., 2010, “Articulated Hybrid Mobile Robot Mechanism With Compounded Mobility and Manipulation and On-Board Wireless Sensor/Actuator Control Interfaces,” *Mechatron. J.*, **20**(6), pp. 627–639.